

Received January 30, 2018, accepted March 14, 2018, date of publication March 28, 2018, date of current version April 23, 2018.

Digital Object Identifier 10.1109/ACCESS.2018.2820043

Spectral–Spatial Hyperspectral Image Classification With K-Nearest Neighbor and Guided Filter

YANHUI GUO^{ID 1,2}, HAN CAO¹, SIMING HAN¹, YUNCHUAN SUN^{ID 3}, (Senior Member, IEEE),

AND YU BAI^{ID 4}, (Member, IEEE)

¹School of Computer Science, Shaanxi Normal University, Xi'an 710119, China

²School of Data and Computer Science, Shandong Women's University, Ji'nan 250300, China

³Business School, Beijing Normal University, Beijing 100875, China

⁴School of Engineering and Computer Science, California State University, Fullerton, CA 92831, USA

Corresponding author: Han Cao (caohan@snnu.edu.cn) and Yunchuan Sun (yunch@bnu.edu.cn)

This work was supported in part by the Natural Science Research Plan in Shaanxi Province under Grant 2016MJ4016, in part by the National Natural Science Foundation of China under Grant 61501287, and in part by the Fundamental Research Funds for the Central Universities of Shaanxi Normal University under Grant GK201703058.

ABSTRACT Explosive growth of applications in hyperspectral image (HSI) has made HSI classification a hot topic in the remote sensing community. The key to improve classification accuracy is how to make full use of the spectral and spatial information. We combine k-nearest neighbor (KNN) algorithm with guided filter which can extract spatial context information and denoise the classification results by edge-preserving filtering. To solve the problem of dimension disaster, we also take dimensionality reduction into account for HSI classification. To verify the feasibility of our proposed methods, we evaluate the performance over four widely used hyperspectral data sets. The experimental results show that with only 5% of samples, our method obtained better performance than improved support vector machine and KNN methods.

INDEX TERMS K-nearest neighbor, guided filter, spectral-spatial hyperspectral image classification.

I. INTRODUCTION

With the development of hyperspectral sensors, hyperspectral images(HSI) are easy to obtain. So, HSI have been widely used in many fields, such as land cover [1], [2], environmental protection [3], agriculture [4], [5], and so on, due to the abundance in spectral and spatial information. HSI classification, as a critical problem for HSI application, has attracted more and more attention.

The goal of HSI classification is to categorize the pixels into one of several classes based on their spectral characteristics. During the last decade, a large number of pixel-wise classifiers were applied, including random forests [6], k-Nearest Neighbor [7], support vector machine(SVM)[8], and sparse representation [9]. However, these traditional methods only focused on the spectral information, ignoring the spatial contextual information which also affected the classification performance. After all, that is a universal phenomenon that remote sensing images exist “different body with same spectrum” or “same body with different spectrum”.

To improve the classification performance further, many researchers proposed spectral-spatial HSI classification which combines spatial context with spectral information, under the assumption that pixels from a local region should have similar spectral information and belong to the same materials. One manner of spectral-spatial classification is based on the kernel combination or fusion, e.g., composite [10], morphological [11], and graphic [12] kernels. The kernel-based methods, especially, in the combination with SVM, have been proved to have good performance in the HSI classification [10]–[12].

In addition, the joint representation model is an effective manner to use spectral and spatial information, drawing on the progress of sparse representation [13] and collaborative representation [14]. The paper [15] exploited a joint sparse model to incorporate the spatial information. The main idea of [15] was that neighboring pixels of a pixel are represented by the sparse samples of training set. Since then, a great deal of literature on sparse models and joint representation has emerged, such as kernel-based joint sparse model [16],

structured joint sparse model [17], dictionary learning [15], [18] and so on. Inspired by the joint representation model, Bo *et al.* [19] develop a novel classification framework based on the Spectral-Spatial K-Nearest Neighbor approach. They exploited the neighbor window of a pixel to represent the spatial information, which effectively applied the abundant spectral-spatial information.

Image filtering has been widely used to suppress or extract content in computer vision, including image restoration, blurring, edge detection, feature extraction, etc. HSI, as a kind of special images, applies edge-preserving filtering(EPF) for hyperspectral image visualization [20]. Early, the joint bilateral filter [21] and the weighted least-squares filter [22] were proposed. Later, the domain transform filter [23] and the guided filter [24] were presented. Among them, the two most widely used are the joint bilateral filter and the guided filter. Motivated by EPF, Kang *et al.* [25] introduced EPFs to spectral-spatial HSI classification. First, they adopted a pixel-wise classifier (support vector machine) to classify each pixel. And then, they applied a EPF to the result classification map, which improved the classification accuracy significantly. The paper [26] also applied guided filter to obtain the spatial feature of HSI. Then, an autoencoder was adopted to extract the feature which combined the spatial information with the spectral information.

Furthermore, deep neural networks have been successfully applied to image classification tasks. Recently, they also have been shown in HSI classification [27]. The papers [28], [29] used an autoencoder to extract spectral features, and followed by a classifier. End-to-end classification based on Convolutional Neural Networks(CNN) [30], [31] was also applied for HSI classification. Since a large number of samples are needed as training set in deep learning(DL) methods, this article does not involve the aforementioned DL methods.

The paper [19] proposed a simple and effective method using KNN with joint model. Although the proposed method has achieved very good results, the classification of the edges is still inaccurate as a result of representing a pixel with its neighbors in a local window. This is mainly because the representation using neighbors makes the edges more obscure. To overcome this problem, we are motivated by the paper [25], which exploited edge-preserving filtering to reserve edge. This paper presents a novel spectral-spatial HSI classification approach with KNN and guided filter, which can solve the above problem.

The remaining parts of this paper are organized as follows. Section II introduces the related methodologies, including K-nearest neighbor, joint representation, and guided filter. Section III proposes two spectral-spatial HSI classification methods, which we called FGF-JKNN and PGF-JKNN. The experiments are given in Section IV. Finally, Section V concludes this paper.

II. RELATED METHODOLOGIES

In this section, we first introduce the principle of KNN. Then, a joint representation model was described for

HSI classification. Finally, we give a detailed description of guided filter.

A. K-NEAREST NEIGHBOR (KNN)

KNN algorithm is a non-parametric method widely used for classification in pattern recognition. The main principle of KNN is that category of a data point is determined according to the classification of the nearest K neighbors. Take $T = \{(x_1, y_1), (x_2, y_2), \dots, (x_N, y_N)\}$ as a training set, and N is the number of training entities. Here $x_i \in R^d$ denotes the feature vectors, and $y_i \in Y = \{c_1, c_2, \dots, c_m\}$ denotes the labels of classification, $i = 1, 2, \dots, N$. Given an input x , we can obtain the k-nearest neighbors $N_k(x)$ by computing the distance with training entities. The voting process is as follows:

$$y = \operatorname{argmax}_{c_j} \sum_{x_i \in N_k(x)} I(y_i = c_j), \quad i = 1, 2, \dots, N \quad (1)$$

where I denotes an indicator function,

$$I = \begin{cases} 1, & y_i = c_j \\ 0, & \text{else.} \end{cases}$$

B. JOINT REPRESENTATION MODEL FOR HSI CLASSIFICATION

In the joint representation model, a basic assumption is that all samples can be represented by the product of the training set and a coefficient matrix. And the coefficient matrix must be sparse. For the HSI data, a local neighbor window of the pixel l tends to share similar characteristic. So, it can be depicted as $Y_l = AX_l$. Where Y_l is a neighbor set, A denotes training set, and X_l is the coefficient matrix. We can compute the coefficient matrix X_l by the following formula.

$$\bar{X}_l = \operatorname{argmin} \|Y_l - AX_l\|_F^2, \quad \text{s.t. } \|X_l\|_{row,0} \leq T_0 \quad (2)$$

After obtaining the coefficient matrix, we can define the distance from Y_l to a special class m as the following.

$$d(Y_l; A^m) = \|Y_l - A^m \bar{X}_l^m\|_F^2 \quad (3)$$

Where the A^m denotes the data set of the class m . Finally, the pixel l is classified the same label with the smallest distance. In this paper, we draw lessons from the joint representation model to obtain a set-to-point distance like the paper [19].

C. GUIDED FILTER

Guided filter was first proposed by He *et al.* [24]. Given a guidance I and an input image p , we can obtain an output image q by guided filter. Generally, q is a linear transform of I in a window ω_k centered at the pixel k . If the radius of k is r , the size of local window ω_k is $(2r + 1) \times (2r + 1)$.

$$q_i = a_k I_i + b_k, \quad \forall i \in \omega_k \quad (4)$$

where a_k is linear coefficient and b_k is a bias. From the model, it is obvious that $\nabla q = a \nabla I$, which means that the filtering output q will have similar edge with guidance image I .

To obtain the coefficient and bias, a minimum cost function in the window ω_k is applied as follows:

$$E(a_k, b_k) = \sum_{i \in \omega_k} ((a_k I_i + b_k - p_i)^2 + \epsilon a_k^2) \quad (5)$$

Here, ϵ is a regularization parameter which could affect the blurring for the guided filter. According to the literal [32], formula (5) leads to a solution as follows.

$$a_k = \frac{\frac{1}{\omega} \sum_{i \in \omega_k} I_i p_i - \mu_k \bar{p}_k}{\sigma_k^2 + \epsilon} \quad (6)$$

$$b_k = \bar{p}_k - a_k \mu_k \quad (7)$$

Where μ_k and σ_k^2 are the mean and variance of I in ω_k , $|\omega|$ is the number of pixels in the local window, and \bar{p}_k is the mean of p in the window. After obtaining the coefficient a_k, b_k , we can compute the filtering output q_i . Through the above process, we can get a linear transform image q .

III. SPECTRAL–SPATIAL HSI CLASSIFICATION WITH KNN AND GUIDED FILTER

The spectral-spatial classification is to classify HSI by the aid of spatial features. Inspired by the paper [26], we firstly extract spatial contextual information of a pixel by guided filter. Then, we exploit KNN proposed by [19] to classify the pixels. Motivated by [25] again, we take spectral-spatial classification as a probability optimization process. The above two methods utilize the idea that the central point can be represented by the surrounding neighbors using guided filter.

A. PROBLEM FORMULATION

Generally, to describe the HSI problem clearly, we define $M = \{\mathbf{x}_1, \mathbf{x}_2, \dots, \mathbf{x}_N\}$ as the hyperspectral data set, where $\mathbf{x}_n = \{x_{n1}, x_{n2}, \dots, x_{nS}\}$ is the n th pixel with S bands, and N denotes the number of HSI pixels. For obtaining a classification, we need to construct a training set $T = \{(\mathbf{x}_1, y_1), (\mathbf{x}_2, y_2), \dots, (\mathbf{x}_M, y_M)\}$, where $y_m \in \{c_1, c_2, \dots, c_K\}$ denotes the one of K labels, and $M < N$ is the number of samples. The aim of HSI classification is to output a y_m for a given $\mathbf{x} \in M$.

B. PROPOSED FGF-WKNN

Due to only taking the spectral information into account, the traditional HSI classification methods perform poorly. How to integrate spatial information and spectral information is the key to improve classification accuracy. Stemming from papers [25], [26], we also employ the guided filter to extract the spatial feature. Our first thought is that the feature embodying the spatial information by guided filter is more suitable for classification. Then, we use KNN to classify the combined feature. The approach we proposed is called as joint representation KNN with front guided filter (FGF-JKNN for short). Concrete scheme is as follows.

First, Principal Component Analysis (PCA) is used to obtain the guidance image G . We take the first principal component as gray-scale guidance image, and take the first three principal components as color guidance image. Given a

data set $D = \{\mathbf{d}_1, \mathbf{d}_2, \dots, \mathbf{d}_S\}$ which is equal to M , we adopt PCA to obtain the following result. Here \mathbf{d}_i is the spatial information of the i th band, and S denotes the number of bands.

$$[\mathbf{p}_1, \dots, \mathbf{p}_S] = PCA(D) \quad (8)$$

So, the gray-scale guidance image is $G = [\mathbf{p}_1]$, first principal component, and the color-scale guidance image is $G = [\mathbf{p}_1, \mathbf{p}_2, \mathbf{p}_3]$.

Then, based on formula (3,4) using input image \mathbf{d}_1 and guidance image G , we can obtain all the parameters $\{a_k, b_k\}$ in the formula (6, 7), and get the filtering output \mathbf{u}_1 . By the same way, we can yield all the \mathbf{d}_i , and construct a new hyperspectral image $U = \{\mathbf{u}_1, \mathbf{u}_2, \dots, \mathbf{u}_S\}$ which has combined the spatial feature with the spectral feature.

Finally, we use a joint representation KNN (JKNN) approach originally presented in [19] to classify the hyperspectral image U . The main idea of JKNN is to represent a pixel with neighbors in a local window of it. Hence, we replace a point-to-point distance with a set-to-point distance, which is expressed by the following:

$$d(N_l; \mathbf{a}_l) = \sum_{0 < j \leq |N_l|} \|\mathbf{n}_j - \mathbf{a}_l\|_2^2 \quad (9)$$

where N_l is the neighbor set of pixel l , \mathbf{a}_l denotes an element of training set, and $|N_l|$ denotes the number of the neighbor set.

C. PROPOSED PGF-JKNN

Different from the above method, motivated by the paper [25], we propose an approach called joint representation KNN with posterior guided filter (PGF-JKNN for short), which takes guided filter as an optimization process after classifying the HSI using JKNN. The specific process is as follows.

First, we adopt JKNN to classify the HSI, and obtain a classification map c . The map c is converted to probability maps $\mathbf{p} = [\mathbf{p}_1, \mathbf{p}_2, \dots, \mathbf{p}_M]$, in which $\mathbf{p}_i = [p_{i1}, p_{i2}, \dots, p_{iN}]$ is a map having the same size of c , and M denotes the number of the category. And $p_{in} = \begin{cases} 1 & \text{if } c_n = i \\ 0 & \text{else} \end{cases}$ is the initial probability that a pixel n belongs to the i -th class.

Then, guided filter is used to filter the probability maps \mathbf{p} . Also, we employed PCA to decompose the initial hyperspectral image D , and obtain the first principal component as guidance image G . The process of yielding guidance image is the same as described in the aforementioned FGF-WKNN.

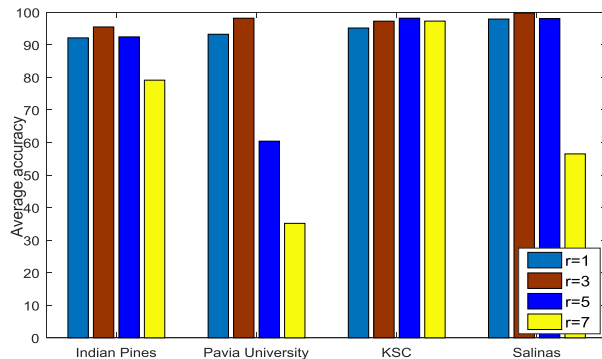
Finally, we choose the maximum probability of each pixel as the classification result. Then, a obtained new classification map \tilde{c} is the final result.

IV. EXPERIMENTS AND RESULTS

In this section, we selected four popular hyperspectral data sets to verify the effectiveness of our proposed methods. And three widely used quality indexes are adopted to evaluate the performance of our methods. Besides, we analyzed the influence factors of this experiments.

TABLE 1. Categories and samples of four data sets.

No.	IndianPines		Pavia University		KSC		Salinas	
	Categories	Samples	Categories	Samples	Categories	Samples	Categories	Samples
C1	Alfalfa	46	Asphalt	6631	Scrub	761	Brocoli_G_W_1	2009
C2	Corn-N	1428	Meadows	18649	Willow swamp	243	Brocoli_G_W_2	3726
C3	Corn-M	830	Gravel	2099	CP hammock	256	Fallow	1976
C4	Corn	237	Trees	3064	CP/Oak	252	Fallow_R_P	1394
C5	Grass-M	483	P-M-sheets	1345	Slash pine	161	Fallow_smooth	2678
C6	Grass-T	730	Bare Soil	5029	Oak/Broadleaf	229	Stubble	3959
C7	Grass-P-M	28	Bitumen	1330	Hardwood swamp	105	Celery	3579
C8	Hay-W	478	S-B-Bricks	3682	Graminoid marsh	431	Grapes_untrained	11271
C9	Oats	20	Shadows	947	Spartina marsh	520	Soil_V_D	6203
C10	Soybean-N	972			Cattail marsh	404	Corn_S_G_W	3278
C11	Soybean-M	2455			Salt marsh	419	Lettuce_R_4wk	1068
C12	Soybean-C	593			Mud flats	503	Lettuce_R_5wk	1927
C13	Wheat	205			Water	927	Lettuce_R_6wk	916
C14	Woods	1265					Lettuce_R_7wk	1070
C15	Build-G-T-D	386					Vinyard_untrained	7268
C16	Stone-S-T	93					Vinyard_V_T	1807
	Total	10249	Total	42776	Total	5211	Total	54129

**FIGURE 1.** Average accuracy for different radius in JKNN.

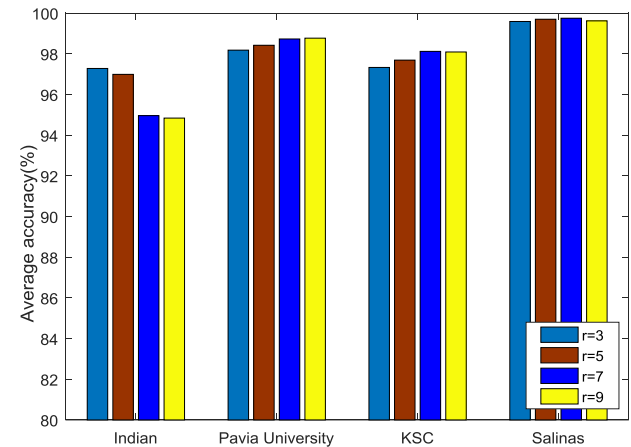
A. EXPERIMENTAL SETUP

1) DATA SETS

There are four hyperspectral data sets used in our experiment, i.e., the Indian Pines, the University of Pavia. The Indian Pines image was recorded by AVIRIS sensor over the Indian Pines test site in North-western Indiana. This image consists of 145×145 pixels with 220 spectral bands in the wavelength range from 0.4 to $2.5 \mu\text{m}$. In this scene, there are 16 categories to be classified, including woods, grass-pasture, and so on.

The University of Pavia image capturing an urban area surrounding the University of Pavia was gathered by the ROSIS03 satellite sensor. The image is composed by 610×340 pixels with 103 spectral bands and a spectral coverage ranging from 0.43 to $0.86 \mu\text{m}$. In this scene, nine classes of interest are considered, such as asphalt, meadows, etc.

Kennedy Space Center(KSC) data set was acquired by AVIRIS, in a range of 224 bands with wavelengths ranging from 0.4 to $2.5 \mu\text{m}$. Given water absorption bands, 176 spectral bands are used for classification. There are 13 different land-cover classes available in this data set, as listed in Table 1.

**FIGURE 2.** Average accuracy for different radius in the guided filter.

Salinas data set was also collected by the AVIRIS sensor, capturing an area over Salinas Valley, California, with a spatial resolution of 3.7m. The image comprises 512×217 pixels with 220 bands. There are 16 different classes which listed in Table 1. We also selected 200 bands for our experiment by removing water absorption bands.

2) EVALUATION METRICS

To evaluate different HSI classification algorithms, we apply three widely used quality indexes, i.e., the overall accuracy (OA), the average accuracy (AA), and the kappa coefficient. OA is the percentage of correctly classified samples to all test samples, AA is the mean of the percentage of correctly classified pixels for each class, and the kappa coefficient is calculated based on the confusion matrix of different classes. Because the samples of training set are randomly selected, we take the average of 10 times experiments as the final result.

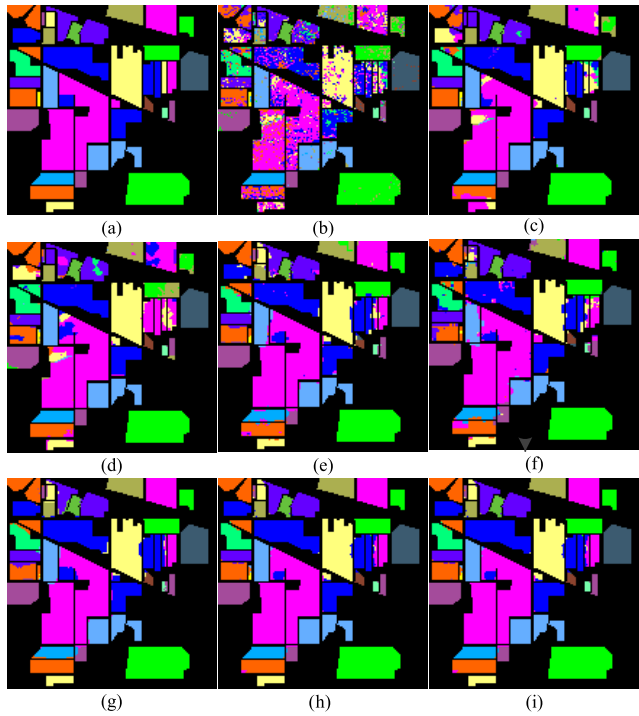


FIGURE 3. Qualitative results of Indian Pines data set. (a) Ground truth. (b) SVM. (c) EPF-g. (d) EPF-c. (e) SSKNN. (f) FGF-JKNN-g. (g) FGF-JKNN-c. (h) PGF-JKNN-g. (i) PGF-JKNN-c.

3) PARAMETER SETTINGS

In our experiment, there are several parameters to be set. The radius r of guided filer and regularization parameter ϵ are the two key factors to affect the result of guided filtering. Radius r is used to express the range of smooth. And ϵ is used to control the ambiguity, in which, the bigger the value, the more blurred the output image is. We set $\epsilon = 0.001$ in this work. Meanwhile, a local window is need to be set for joint representation KNN. We also set the r of the local window to 3. For the above four datasets, we take 5% of the data as the training set and the remaining 95% to test the proposed approach.

B. INFLUENCE FACTORS OF EXPERIMENTS

1) ANALYSIS ON PARAMETERS OF KNN

Motivated by the joint representation model, we adopt a set-to-point distance instead of point-to-point distance in the KNN. The set consists of pixels in a local window of a pixel. The radius of the window is a factor to influence the classification accuracy. We set a radius of 1, 3, 5, 7, respectively, for all the data sets. The average accuracy in ten times was shown in Figure 1. We can see that, except for KSC, the accuracy of data sets is the highest when the radius is 3. So, we choose a radius of 3 as an experimental parameter.

2) INFLUENCE OF GUIDED FILTER PARAMETER

The radius of guided filter which means the scale of spatial information also is a key factor to affect HSI classification accuracy. We set a radius of 3, 5, 7, and 9 for all the four data

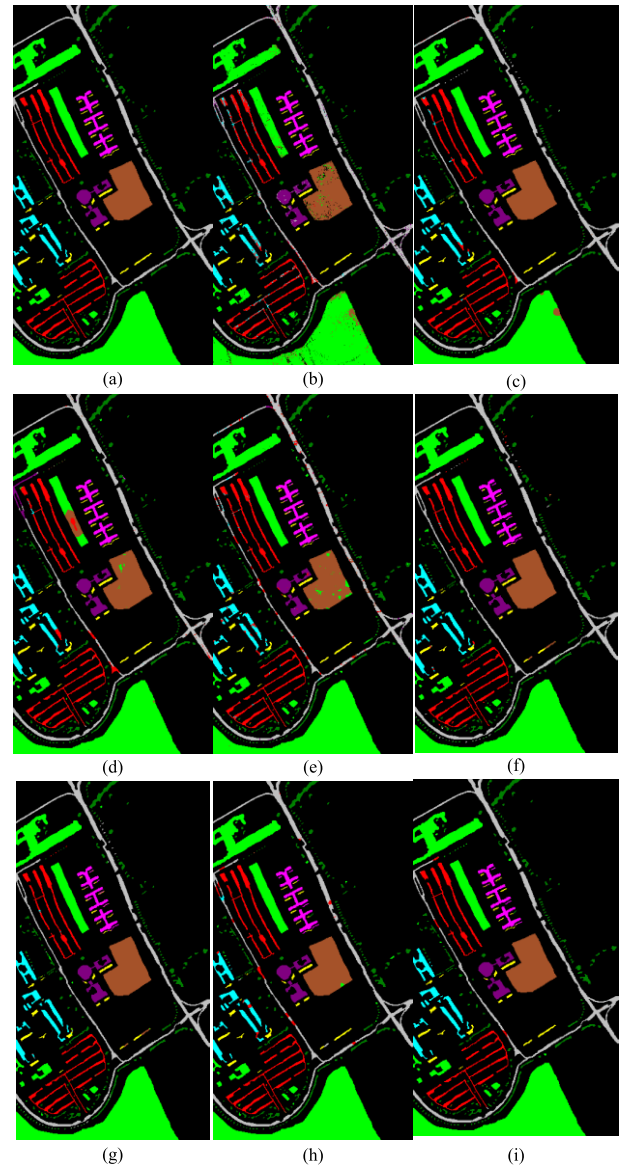


FIGURE 4. Qualitative results of University of Pavia data set. (a) Ground truth. (b) SVM. (c) EPF-g. (d) EPF-c. (e) SSKNN. (f) FGF-JKNN-g. (g) FGF-JKNN-c. (h) PGF-JKNN-g. (i) PGF-JKNN-c.

sets, respectively. Figure 2 shows the average classification results of the four data sets. The radius of guided filter in our experiments are 3, 7, 9, 7 for Indian Pines, University of Pavia, KSC, and Salinas, respectively.

3) INFLUENCE OF DIMENSIONALITY REDUCTION

Considerable literature shows that high dimension will cause the Hughes phenomenon. Many researchers adopted principal component analysis (PCA) and independent component analysis (ICA) to reduce the dimension. So, in this paper, we take Indian Pines data set as an example, and discuss the effect of dimensionality reduction on the HSI classification accuracy. We reduced the dimension of Indian to 150, 100, 50 by PCA, respectively. And corresponding results are 96.81%, 96.80%, and 96.69%, respectively.

TABLE 2. Classification accuracy on the indian pines data set (5% samples for training).

Categories	SVM [8]	EPF-g [25]	EPF-c [25]	SSKNN [19]	FGF- JKNN-g	FGF- JKNN-c	PGF- JKNN-g	PGF- JKNN-c
C1	45.16	100.00	100.00	100.00	100.00	100.00	100.00	100.00
C2	63.35	96.00	82.44	93.06	93.83	92.11	98.87	96.48
C3	55.60	90.34	77.33	93.77	91.50	93.47	97.70	98.10
C4	39.43	61.82	100.00	100.00	94.69	100.00	96.88	99.55
C5	85.68	97.01	96.60	93.90	87.94	95.00	99.32	98.89
C6	92.31	97.90	100.00	95.86	95.70	96.70	98.44	98.86
C7	55.56	100.00	92.86	95.45	100.00	100.00	100.00	100.00
C8	93.56	97.59	100.00	98.06	97.63	100.00	100.00	99.78
C9	77.78	100.00	70.00	100.00	100.00	100.00	100.00	100.00
C10	61.46	71.74	85.11	91.24	93.84	95.89	96.49	95.83
C11	75.99	92.26	93.14	93.40	91.55	98.05	98.24	96.11
C12	50.16	84.87	94.27	93.88	84.39	93.06	95.39	98.38
C13	87.18	100.00	100.00	92.51	88.89	94.30	100.00	98.48
C14	94.19	99.40	96.69	97.06	98.36	99.75	98.61	100.00
C15	54.77	89.74	95.60	96.63	99.68	98.61	99.72	99.73
C16	97.78	79.31	100.00	98.72	100.00	89.89	96.63	100.00
OA	71.73	90.52	91.33	94.38	93.22	96.28	98.19	98.76
AA	70.62	91.12	92.75	95.85	94.87	96.68	98.52	97.73
KA	67.78	89.14	90.01	93.59	92.27	95.76	97.94	97.41

TABLE 3. Classification accuracy on university of pavia data set (5% samples for training).

Categories	SVM [8]	EPF-g [25]	EPF-c [25]	SSKNN [19]	FGF- JKNN-g	FGF- JKNN-c	PGF- JKNN-g	PGF- JKNN-c
C1	94.01	99.30	99.64	99.77	98.13	98.31	99.82	99.92
C2	96.33	99.30	99.65	97.85	99.14	99.69	99.04	99.43
C3	87.51	94.84	95.70	93.14	97.79	98.71	98.74	99.40
C4	98.24	96.28	99.02	97.85	96.52	97.98	98.99	99.15
C5	100.00	100.00	100.00	94.71	93.21	91.81	95.16	95.23
C6	96.30	100.00	100.00	97.24	99.81	98.37	99.85	100.00
C7	91.63	100.00	100.00	94.01	96.86	98.52	97.98	100.00
C8	89.61	99.08	99.40	85.30	93.99	97.17	92.12	97.43
C9	100.00	99.79	100.00	98.72	99.85	99.22	100.00	100.00
OA	95.30	99.09	99.53	96.36	98.10	98.62	98.44	99.26
AA	94.85	98.73	99.27	95.40	97.26	97.75	97.97	99.03
KA	93.31	98.68	99.32	95.17	97.48	98.17	97.94	98.95

All of them are inferior to the result of 200. Hence, we do not use dimensionality reduction in our experiments.

C. EXPERIMENTAL RESULTS

In this section, we compare our proposed methods (FGF-JKNN-g, FGF-JKNN-c, PGF-JKNN-g, PGF-JKNN-c) with several widely used HSI classification methods, including the method based on SVM [8], EPF [25], and SSKNN [19]. The abbreviations g or c denote gray guidance filter and color guidance filter, which are obtained by the first principal component or the first three components, respectively.

1) EXPERIMENT ON INDIAN PINES DATA SET

To evaluate our methods, we compared the performance of the methods using the quantitative index of OA, AA and KA. The experimental results are shown in Figure 3 and Table 2. We can see from Figure 3, that the last two pictures are

similar to ground truth, and SSKNN performs poorly on edge pixels.

From the detailed results in Table 2, we also see that there is a vast gap between the pixel-wise classifier (SVM, which is an outstanding classifier) and spectral-spatial classifier. Our proposed FGF-JKNN-c and PGF-JKNN outperform EPF and SSKNN methods. Especially, PGF-JKNN increased 4% and 8%, compared to SSKNN and EPF, respectively.

From this experiment, we can draw the following conclusion. a) Guided filter can overcome the classification inaccuracy of edge pixels in SSKNN. b) KNN with posterior guided filter is more useful than that with front guided filter. c) Color guided filter is more effective than gray guided filter.

2) EXPERIMENT ON UNIVERSITY OF PAVIA DATA SET

The second experiment is performed on the University of Pavia. Figure 4 shows the classification maps obtained by

TABLE 4. Classification accuracy on the KSC data set (5% samples for training).

Categories	SVM [8]	EPF-g [25]	EPF-c [25]	SSKNN [19]	FGF- JKNN-g	FGF- JKNN-c	PGF- JKNN-g	PGF- JKNN-c
C1	93.90	100.00	100.00	98.14	99.73	100.00	99.06	100.00
C2	87.68	100.00	100.00	99.10	100.00	100.00	98.67	100.00
C3	90.04	100.00	100.00	85.82	100.00	95.55	100.00	97.51
C4	62.61	100.00	97.81	100.00	85.61	98.72	91.70	97.89
C5	60.00	88.68	93.79	100.00	100.00	97.92	100.00	100.00
C6	63.06	100.00	100.00	99.52	96.31	97.21	100.00	100.00
C7	71.93	91.40	100.00	96.59	98.84	100.00	100.00	100.00
C8	79.35	100.00	100.00	100.00	99.45	100.00	100.00	99.76
C9	88.75	100.00	100.00	93.46	100.00	100.00	100.00	100.00
C10	95.97	100.00	100.00	95.73	97.71	100.00	100.00	100.00
C11	82.26	93.66	100.00	99.75	100.00	100.00	100.00	100.00
C12	98.25	100.00	100.00	100.00	100.00	100.00	100.00	100.00
C13	100.00	100.00	100.00	97.53	97.53	99.89	100.00	100.00
OA	87.66	98.93	99.72	97.27	98.30	99.52	99.37	99.76
AA	82.60	97.98	99.35	97.36	98.09	99.18	99.19	99.63
KA	86.24	98.80	99.68	96.96	98.11	99.46	99.30	99.73

TABLE 5. Classification accuracy on the salinas data set (5% samples for training).

Categories	SVM [8]	EPF-g [25]	EPF-c [25]	SSKNN [19]	FGF- JKNN-g	FGF- JKNN-c	PGF- JKNN-g	PGF- JKNN-c
C1	99.89	100.00	100.00	100.00	100.00	100.00	100.00	100.00
C2	99.61	100.00	100.00	100.00	100.00	100.00	100.00	100.00
C3	97.30	98.91	99.39	99.78	100.00	100.00	100.00	100.00
C4	97.29	98.24	98.24	94.80	96.98	96.98	98.79	98.39
C5	98.64	99.88	99.96	99.47	99.80	99.76	100.00	100.00
C6	100.00	100.00	100.00	99.60	100.00	100.00	100.00	100.00
C7	99.36	100.00	100.00	99.85	99.30	99.30	100.00	100.00
C8	81.23	92.91	94.95	95.82	100.00	100.00	99.79	100.00
C9	99.26	100.00	100.00	99.98	100.00	100.00	100.00	100.00
C10	90.38	96.73	97.32	99.97	99.94	100.00	100.00	99.97
C11	95.90	98.36	99.12	99.01	99.67	99.67	100.00	100.00
C12	97.23	100.00	100.00	100.00	100.00	99.94	100.00	100.00
C13	98.02	100.00	100.00	99.87	99.20	99.47	100.00	100.00
C14	95.74	99.78	100.00	98.04	98.89	98.79	99.56	100.00
C15	70.77	91.23	92.24	93.96	100.00	100.00	99.03	96.78
C16	99.69	100.00	100.00	100.00	100.00	100.00	100.00	100.00
OA	90.71	96.95	97.60	98.00	99.83	99.83	99.78	99.90
AA	95.02	98.50	98.83	98.76	99.61	99.62	99.82	99.85
KA	89.62	96.59	97.32	97.77	99.81	99.81	99.76	99.89

different methods. From this figure, it can be seen that the classification obtained by the SVM and SSKNN is not very satisfactory since some noisy are still visible. The classification accuracy of EPF-c, FGF-JKNN-g, PGF-JKNN-g is roughly the same. From the result in Table 3, we can observe that the performance of SVM has improved greatly in all quality indexes, compared with the classification in the Indian Pines data set. Maybe the reason is that SVM classifier is not suitable for multiclass problem. Due to the small number of classes in the University of Pavia, the EPF-g and EPF-c are slightly better than our proposed methods. However, compared to the primary reference approach SSKNN, all our methods have increased by nearly 3%, in the OA, AA, and KA.

3) EXPERIMENT ON KSC DATA SET

In the KSC data set, the vast majority of pixels are in the background, and only 5000 pixels are used to train and test. That is, it has the characteristic of small sample and high dimension. The following Figure 5 shows the classification results of KSC data set. In Figure 5, we can see that only the result of SVM has some noises compared with ground truth.

The detailed classification results are shown in Table 4. From the Table 6, we can see that the top three accuracy are PGF-JKNN-c, EPF-c, and FGF-JKNN-c, all of which adopt color guided filter to extract spatial information. That is, color guided filter is more effective than gray guided filter, which coincides with the conclusion of the previous experiment. SSKNN is the worst one of spectral-spatial HSI classification

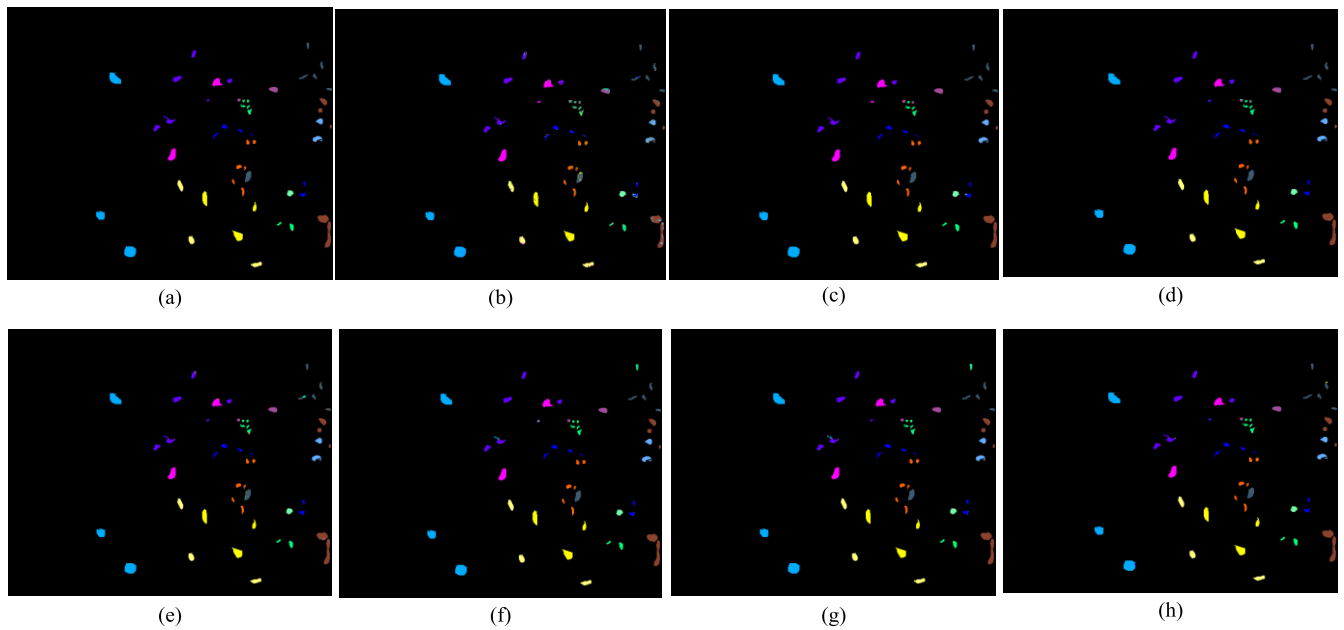


FIGURE 5. Qualitative results of KSC data set. (a) Ground truth. (b) SVM. (c) EPF-g. (d) EPF-c. (e) SSKNN. (f) FGF-JKNN-g. (g) FGF-JKNN-c. (h) PGF-JKNN-g.

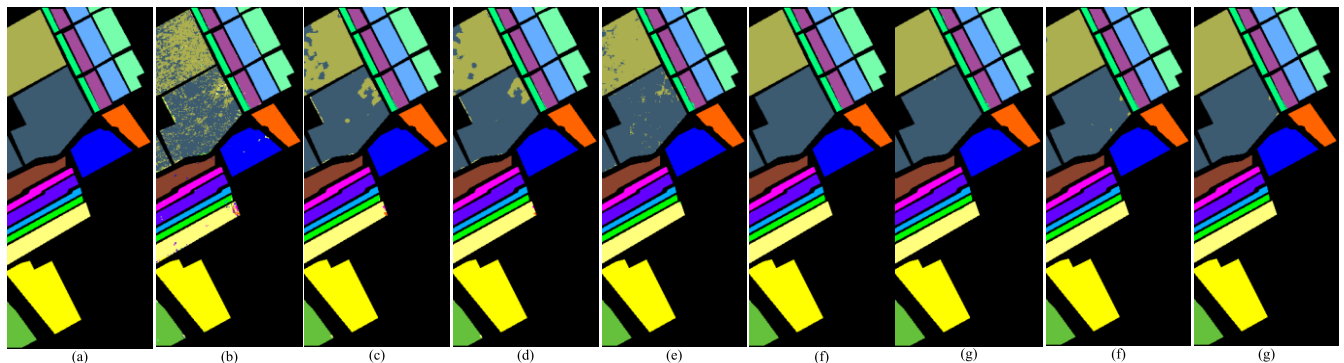


FIGURE 6. Qualitative results Salinas data set. (a) Ground truth. (b) SVM. (c) EPF-g. (d) EPF-c. (e) SSKNN. (f) FGF-JKNN-g. (g) FGF-JKNN-c. (h) PGF-JKNN-g. (i) PGF-JKNN-c.

methods. That means that SSKNN is not suitable for data set with small samples.

4) EXPERIMENT ON SALINAS DATA SET

There are more than 50,000 samples in Salinas data set, which is the biggest one we have chosen. The category of Salinas has regular shape, which is helpful to classify. The classification results are shown in Figure 6 and Table 5.

From the figure 6, we can see that the result map of SVM has many noise points which were set wrong labels. All of our proposed methods outperform other metods (EPF, SSKNN), and obtain the accuracy beyond 99%.

Table 5 illustrates the detailed classification accuracy. Compared with SVM and EPF, our proposed methods (FGF-JKNN, GFG-JKNN) increase by 1% and 3%, respectively. Especially, PGF-JKNN-c got a dramatic 99.9%, which outperforms state-of-the-art methods.

Comparing the methods on the four data sets, we can observe that our proposed methods are better than other methods in three data sets (Indian Pines, KSC, and Salinas) except for University of Pavia data set. University of Pavia data set has the characteristics of few categories and low dimension, which are more suitable for SVM classifier. SSKNN method performs poorly on KSC data set. That is because SSKNN is more fitable for regular shapes and large scale shapes. Our proposed FPF-JKNN and GPF-JKNN are more robust to solve complex problems.

V. CONCLUSION

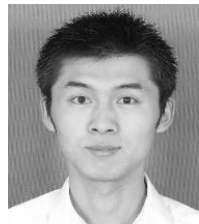
In this paper, we proposed two novel spectral-spatial HSI classification methods which combines joint representation KNN with guided filter. A front guided filter method is used to extract spatial information. A posterior guided filter take advantage of denoising to optimize the classification result.

The proposed two methods perform well and succeeded in classifying hyperspectral images with highest accuracies, especially compared to our primary reference object SSKNN.

From this work, we can draw the following conclusions. a) Dimension reduction is not necessary for HSI classification. b) Guided filter can extract the spatial information of HSI effectively, and classify the edge pixels of HSI more accurately. c) For different data sets, the radius of guided filter should be different, to get a better classification result. d) Color guided filter is more effective than gray guided filter.¹

REFERENCES

- [1] R. J. Zomer, A. Trabucco, and S. L. Ustin, "Building spectral libraries for wetlands land cover classification and hyperspectral remote sensing," *J. Environ. Manage.*, vol. 90, no. 7, pp. 2170–2177, 2009.
- [2] G. P. Petropoulos, C. Kalaitzidis, and K. P. Vadrevu, "Support vector machines and object-based classification for obtaining land-use/cover cartography from hyperion hyperspectral imagery," *Comput. Geosci.*, vol. 41, pp. 99–107, Apr. 2012.
- [3] R. L. Lawrence, S. D. Wood, and R. L. Sheley, "Mapping invasive plants using hyperspectral imagery and Breiman Cutler classifications (Random Forest)," *Remote Sens. Environ.*, vol. 100, no. 3, pp. 356–362, 2006.
- [4] L. M. Dale et al., "Hyperspectral imaging applications in agriculture and agro-food product quality and safety control: A review," *Appl. Spectrosc. Rev.*, vol. 48, no. 2, pp. 142–159, 2013.
- [5] D. Haboudane, J. R. Miller, E. Pattey, P. J. Zarco-Tejada, and I. B. Strachan, "Hyperspectral vegetation indices and novel algorithms for predicting green LAI of crop canopies: Modeling and validation in the context of precision agriculture," *Remote Sens. Environ.*, vol. 90, no. 3, pp. 337–352, 2004.
- [6] M. Dalponte, H. O. Orka, T. Gobakken, D. Gianelle, and E. Naesset, "Tree species classification in boreal forests with hyperspectral data," *IEEE Trans. Geosci. Remote Sens.*, vol. 51, no. 5, pp. 2632–2645, May 2013.
- [7] L. Ma, M. M. Crawford, and J. Tian, "Local manifold learning-based k -nearest-neighbor for hyperspectral image classification," *IEEE Trans. Geosci. Remote Sens.*, vol. 48, no. 11, pp. 4099–4109, Nov. 2010.
- [8] F. Melgani and L. Bruzzone, "Classification of hyperspectral remote sensing images with support vector machines," *IEEE Trans. Geosci. Remote Sens.*, vol. 42, no. 8, pp. 1778–1790, Aug. 2004.
- [9] Y. Chen, N. M. Nasrabadi, and T. D. Tran, "Hyperspectral image classification via kernel sparse representation," *IEEE Trans. Geosci. Remote Sens.*, vol. 51, no. 1, pp. 217–231, Jan. 2013.
- [10] G. Camps-Valls, L. Gomez-Chova, J. Munoz-Mari, J. Vila-Frances, and J. Calpe-Maravilla, "Composite kernels for hyperspectral image classification," *IEEE Geosci. Remote Sens. Lett.*, vol. 3, no. 1, pp. 93–97, Jan. 2006.
- [11] M. Fauvel, J. Chanussot, and J. A. Benediktsson, "A spatial-spectral kernel-based approach for the classification of remote-sensing images," *Pattern Recognit.*, vol. 45, no. 1, pp. 381–392, 2012.
- [12] G. Camps-Valls, N. Shervashidze, and K. M. Borgwardt, "Spatio-spectral remote sensing image classification with graph kernels," *IEEE Geosci. Remote Sens. Lett.*, vol. 7, no. 4, pp. 741–745, Oct. 2010.
- [13] J. Wright, A. Y. Yang, A. Ganesh, S. S. Sastry, and Y. Ma, "Robust face recognition via sparse representation," *IEEE Trans. Pattern Anal. Mach. Intell.*, vol. 31, no. 2, pp. 210–227, Feb. 2009.
- [14] L. Zhang, M. Yang, and X. Feng, "Sparse representation or collaborative representation: Which helps face recognition?" in *Proc. IEEE Int. Conf. Comput. Vis. (ICCV)*, Nov. 2011, pp. 471–478.
- [15] Y. Chen, N. M. Nasrabadi, and T. D. Tran, "Hyperspectral image classification using dictionary-based sparse representation," *IEEE Trans. Geosci. Remote Sens.*, vol. 49, no. 10, pp. 3973–3985, Oct. 2011.
- [16] J. Liu, Z. Wu, Z. Wei, and L. Xiao, "Hyperspectral image classification using kernel sparse representation and semilocal spatial graph regularization," *IEEE Geosci. Remote Sens. Lett.*, vol. 11, no. 8, pp. 1320–1324, Sep. 2014.
- [17] X. Sun, Q. Qu, N. M. Nasrabadi, and T. D. Tran, "Structured priors for sparse-representation-based hyperspectral image classification," *IEEE Geosci. Remote Sens. Lett.*, vol. 11, no. 7, pp. 1235–1239, Dec. 2013.
- [18] A. Soltani-Farani, H. R. Rabiee, and S. A. Hosseini, "Spatial-aware dictionary learning for hyperspectral image classification," *IEEE Trans. Geosci. Remote Sens.*, vol. 53, no. 1, pp. 527–541, Jan. 2015.
- [19] C. Bo, H. Lu, and D. Wang, "Spectral-spatial K-nearest neighbor approach for hyperspectral image classification," *Multimedia Tools Appl.*, vol. 8, pp. 1–18, 2017.
- [20] K. Kotwal and S. Chaudhuri, "Visualization of hyperspectral images using bilateral filtering," *IEEE Trans. Geosci. Remote Sens.*, vol. 48, no. 5, pp. 2308–2316, May 2010.
- [21] C. Tomasi and R. Manduchi, "Bilateral filtering for gray and color images," in *Proc. 6th Int. Conf. Comput. Vis.*, Jan. 1998, pp. 839–846.
- [22] Z. Farbman, D. Lischinski, and R. Szeliski, "Edge-preserving decompositions for multi-scale tone and detail manipulation," *Trans. Graph.*, vol. 27, no. 3, p. 67, Aug. 2008.
- [23] E. S. L. Gastal and M. M. Oliveira, "Domain transform for edge-aware image and video processing," *ACM Trans. Graph.*, vol. 30, no. 4, p. 69, 2011.
- [24] K. He, J. Sun, and X. Tang, "Guided image filtering," *IEEE Trans. Pattern Anal. Mach. Intell.*, vol. 35, no. 6, pp. 1397–1409, Jun. 2013.
- [25] X. Kang, S. Li, and J. A. Benediktsson, "Spectral-spatial hyperspectral image classification with edge-preserving filtering," *IEEE Trans. Geosci. Remote Sens.*, vol. 52, no. 5, pp. 2666–2677, May 2014.
- [26] L. Wang, J. Zhang, P. Liu, K.-K. R. Choo, and F. Huang, "Spectral-spatial multi-feature-based deep learning for hyperspectral remote sensing image classification," *Soft Comput.*, vol. 21, no. 1, pp. 213–221, 2017.
- [27] L. Zhang, L. Zhang, and B. Du, "Deep learning for remote sensing data: A technical tutorial on the state of the art," *IEEE Geosci. Remote Sens. Mag.*, vol. 4, no. 2, pp. 22–40, Jun. 2016.
- [28] X. Ma, H. Wang, and J. Geng, "Spectral-spatial classification of hyperspectral image based on deep auto-encoder," *IEEE J. Sel. Topics Appl. Earth Observ. Remote Sens.*, vol. 9, no. 9, pp. 4073–4085, Sep. 2016.
- [29] Z. Lin, Y. Chen, X. Zhao, and G. Wang, "Spectral-spatial classification of hyperspectral image using autoencoders," in *Proc. 9th Int. Conf. IEEE Inf. Commun. Signal Process. (ICICS)*, Dec. 2013, pp. 1–5.
- [30] S. Yu, S. Jia, and C. Xu, "Convolutional neural networks for hyperspectral image classification," *Neurocomputing*, vol. 219, pp. 88–98, Jan. 2017.
- [31] Y. Chen, H. Jiang, C. Li, X. Jia, and P. Ghamisi, "Deep feature extraction and classification of hyperspectral images based on convolutional neural networks," *IEEE Trans. Geosci. Remote Sens.*, vol. 54, no. 10, pp. 6232–6251, Oct. 2016.
- [32] J. Friedman, T. Hastie, and R. Tibshirani, *The Elements of Statistical Learning*. Berlin, Germany: Springer, 2001.



YANHUI GUO received the B.S. degree in information management and information system from the Xi'an University of Finance and Economics, Xi'an, China, in 2006, and the M.S. degree in computer software and theory from Shaanxi Normal University, Xi'an, in 2009, where he is currently pursuing the Ph.D. degree with the School of Computer Science.

Since 2009, he has been with the School of Information Technology, Shandong Women's University, Ji'nan, China, where he is currently a Senior Lecturer. His research interests include data mining, machine learning, and remote sensing image process.



HAN CAO received the B.S. degree from Northwest University, Xi'an, China, in 1989, and the Ph.D. degree from the State Key Laboratory of Information Engineering in Surveying, Mapping, and Remote Sensing, Wuhan University, Wuhan, China, in 2002.

Since 1989, she has been with the School of Computer Science, Shaanxi Normal University, Xi'an, where she is currently a Professor. She has authored or co-authored over 170 referred papers, including 68 journal papers. She has authored or co-authored over 70 referred papers. Her research interests include pattern recognition, remote sensing, tourism demand forecasting, and spatial data analysis.

¹*Authors contributed equally



SIMING HAN received the B.S. degree from the National Pilot School of Software, Yunnan University, Kunming, China, in 2014. He is currently pursuing the M.S. degree with the School of Computer Science, Shaanxi Normal University, Xi'an, China.

His research interests include data mining and machine learning.



YU BAI received the B.S. degree in electrical engineering from Ukraine National Aviation University in 2008, the M.S. degree in electrical and computer engineering from the University of Texas Pan American in 2011, and the Ph.D. degree in electrical engineering from the University of Central Florida in 2016. He is currently an Assistant Professor with the Computer Engineering Program, College of Engineering and Computer Science, California State University, Fullerton, CA, USA. Prior to his academic career, he had been at Siemens Energy Inc.

His research interests include stochastic computing, neuromorphic computing, FPGA design, nano-scale computing system with novel silicon and post-silicon devices, and low power digital and mixed-signal CMOS circuit design.



YUNCHUAN SUN (SM'16) received the Ph.D. degree from the Institute of Computing Technology, Chinese Academy of Sciences, in 2009. He is currently a Professor with the Business School, Beijing Normal University. His research interests include big data, IoT, semantic technologies, and information security.

He is the Secretary of the IEEE Communications Society IoT Technical Subcommittee, an Active Chair of ETTC TF on SmartWorld at IEEE CIS, an Associate Editor of *Personal and Ubiquitous Computing*, and a Founder of IIKI series events.